

Optimization of selective powder deposition for multi-material powder bed fusion: process innovations and applications

Simon Girnth, Christian Wacker, Nils Waldt, Günter Klawitter, Klaus Dröder

Suggested citation:

Girnth, Simon, Christian Wacker, Nils Waldt, Günter Klawitter, and Klaus Dröder. 2025. "Optimization of selective powder deposition for multi-material powder bed fusion: process innovations and applications." *Progress in Additive Manufacturing* 10 (8): 5367–85. <https://doi.org/10.25968/opus-3457>.

Abstract

Additive manufacturing processes based on powder bed fusion offer a high degree of design flexibility and enable the processing of a wide range of materials, including metals, ceramics, and polymers, while maintaining minimal porosity. However, production of multi-material components with locally tailored properties to meet specific requirements by incorporating different materials with a high degree of spatial selectivity remains an elusive challenge. Essential prerequisites for achieving this selectivity are specialized selective powder deposition techniques, their development, characterization, and subsequent implementation. In order to investigate optimization potentials and to identify research gaps in the field of selective powder deposition techniques, an evaluation of the current literature is performed in this study, ultimately highlighting promising potentials for vibration-assisted approaches. Key considerations include the reduction of implementation complexity and the downscaling of associated devices to increase their applicability. To achieve implementation simplification, this study derives dimensionless quantities that facilitate a targeted calculation of control parameters by associating powder layer quality metrics with relevant input quantities. The validity of the derived dimensionless quantities is verified by discrete-element method simulations and physical experiments employing a novel miniaturized vibration-assisted device. Metal, ceramic and polymer powders are used as representative samples to demonstrate the versatility of the method for different classes of materials. Ultimately, the presented methods enable a significant improvement in the applicability of vibration-assisted devices and represent an integrative component that provides a suitable basis for further research efforts in the field of combined processing of multiple materials by additive manufacturing technologies that utilize powder beds.

Terms of use

CC BY 4.0



Optimization of selective powder deposition for multi-material powder bed fusion: process innovations and applications

Simon Girnth¹ · Christian Wacker² · Nils Waldt¹ · Günter Klawitter¹ · Klaus Dröder²

Received: 6 October 2024 / Accepted: 2 December 2024 / Published online: 17 December 2024
© The Author(s) 2024

Abstract

Additive manufacturing processes based on powder bed fusion offer a high degree of design flexibility and enable the processing of a wide range of materials, including metals, ceramics, and polymers, while maintaining minimal porosity. However, production of multi-material components with locally tailored properties to meet specific requirements by incorporating different materials with a high degree of spatial selectivity remains an elusive challenge. Essential prerequisites for achieving this selectivity are specialized selective powder deposition techniques, their development, characterization, and subsequent implementation. In order to investigate optimization potentials and to identify research gaps in the field of selective powder deposition techniques, an evaluation of the current literature is performed in this study, ultimately highlighting promising potentials for vibration-assisted approaches. Key considerations include the reduction of implementation complexity and the downscaling of associated devices to increase their applicability. To achieve implementation simplification, this study derives dimensionless quantities that facilitate a targeted calculation of control parameters by associating powder layer quality metrics with relevant input quantities. The validity of the derived dimensionless quantities is verified by discrete-element method simulations and physical experiments employing a novel miniaturized vibration-assisted device. Metal, ceramic and polymer powders are used as representative samples to demonstrate the versatility of the method for different classes of materials. Ultimately, the presented methods enable a significant improvement in the applicability of vibration-assisted devices and represent an integrative component that provides a suitable basis for further research efforts in the field of combined processing of multiple materials by additive manufacturing technologies that utilize powder beds.

Keywords Selective powder deposition · Multi-material · Discrete-element method · Pi theorem · Dimensionless numbers

1 Introduction

Additive manufacturing (AM) offers unique advantages such as cost-effective small-scale production, increased design flexibility and material efficiency. In particular, powder bed fusion using laser beam (PBF-LB) has become established in the additive processing of metals, primarily due to its ability to produce dimensionally accurate structures with intricate topology. Recently, there has been growing interest in the multi-material capability of PBF-LB [1–3], which could further expand its applicability by enabling the production of parts with locally tailored properties [4].

However, multi-material processing in PBF-LB poses significant challenges for machine technology and process control [5]. These range from ensuring material compatibility and controlling complex thermal dynamics [6, 7] to developing sophisticated selective powder deposition (SPD) techniques to achieve spatial material selectivity within the

✉ Simon Girnth
simon.girnth@hs-hannover.de

Christian Wacker
c.wacker@tu-braunschweig.de

Nils Waldt
nils.waldt@hs-hannover.de

Günter Klawitter
guenter.klawitter@hs-hannover.de

Klaus Dröder
k.droeder@tu-braunschweig.de

¹ Faculty II, Hochschule Hannover, University of Applied Sciences and Arts, 30459 Hannover, Germany

² Institute for Machine Tools and Production Technology, Technische Universität Braunschweig, 38106 Braunschweig, Germany

powder bed [2, 8, 9]. However, successful application of SPD requires knowledge of the relationships between the relevant influences and the resulting powder bed quality (relative density, homogeneity, etc.), which affects the quality of the solidified volume [10].

In addition to physical experiments, process virtualization is increasingly being used to determine possible correlations [11–13]. These enable the independent variation and optimization of both state and process variables over a wide range of spatial scales, including those used in PBF-powders. In this context, the use of the discrete-element method (DEM) is particularly advantageous for investigations in which the results are directly derived from the properties of the powder particles, e.g., particle size distribution, shape and mechanical properties. This is especially important when geometric constraints preclude a continuum approach. Taking these limitations into account, DEM facilitates the analysis of mechanisms influencing powder deposition in powder bed additive manufacturing, since the typical layer thicknesses, which range from about 20 to 100 μm , correspond to average grain diameters [14–19].

In the following sections of this study, the DEM is first used to investigate the influence of control parameters and other governing variables on the resulting quality metrics with respect to powder bed additive manufacturing. The evaluation is based on dimensionless quantities derived in this study that summarize the governing variables and establish a mathematical link to the process outcome. The simulated results are then validated experimentally using a novel vibrating SPD device that demonstrates the ability to process various metal, ceramic and polymer powders. A key advantage of the novel vibrating SPD device presented here over the current state of the art is its significantly reduced size, which is achieved by its realization as an additively manufactured integral component. Finally, the results of both the virtual and physical experiments will be combined into a novel application method that facilitates the use of vibration-assisted SPD. This is achieved for the first time on the basis of dimensionless quantities.

2 Methods for the preparation of material-selective powder layers

For the preparation of powder layers with locally different material compositions, various approaches are available in the literature. Depending on the functional principle and technological maturity, they currently offer different degrees of applicability [8] and potentials for research and development. In this context, prevalent approaches are discussed in order to elucidate distinct potentials and to identify research gaps. Therefore, an evaluation framework including metrics

for determining the resulting powder layer quality as well as the operability of SPD devices is presented and applied.

2.1 Evaluation framework for applicability of SPD approaches

The evaluation framework (Fig. 1) considers particle and bulk properties in conjunction with the applied SPD approaches as elements determining the resulting dimensions of applicability, thus enabling its assessment. The dimensions of applicability of SPD approaches are primarily determined by the operability and resulting properties of the powder layer. In the following operability is used to refer to a set of characteristics, which determine the performance, efficiency, precision and reliability of the process. Important considerations include process speed, precision and resolution of material selectivity, ability to compensate for substrate irregularities, flexibility in material selection, system complexity, robustness and reliability as well as ease of powder management and previous powder conditioning requirements. In this context, production efficiency is primarily determined by the deposition rate. Therefore, its maximization is an integral aspect of ensuring the economic viability of SPD. The precision and resolution of material selectivity determines the discretization error, which occurs when zones of varied powder compositions are implemented within a layer. The next aspect is the ability to compensate for irregularities, which include variations in substrate topography caused by phenomena such as denudation effects or pronounced melt pool dynamics. Another measure of the operability of SPD devices is the absence of constraints related to the physical and morphological properties of the powder, thus providing high material flexibility. Finally, the complexity and robustness of the system determine the susceptibility to failure, maintenance effort as well as the uptime, which affects the overall economic feasibility of the system. High operability is, therefore, achieved when the system efficiently and precisely achieves the desired results and meets the requirements for flexibility and robustness with manageable complexity.

The quality of the powder layer can be described based on the criteria of layer thickness, void volume fraction [14, 16, 19–23], homogeneity [13, 14, 18, 20, 21, 23], material composition, and contamination [24, 25]. It correlates with the quality criteria of PBF-LB components, which include surface quality, dimensional accuracy, porosity, and mechanical properties [10]. The linking of these quality criteria for both individual layers and the final part results from complex interactions during the solidification process, such as laser energy coupling, heat transfer as well as the phase transition behavior of the material [26]. The quality of powder layers is, therefore, of crucial importance for achieving the

Determining process elements	Particle & bulk properties	<ul style="list-style-type: none"> • Morphology (particle size, roundness, sphericity etc.) • Resulting/ bulk properties (tap density, Hausner ratio, flowability etc.) • Physical properties (Young’s modulus, surface energy density etc.) • Chemical properties (composition, hydrophilicity etc.) • Electrostatic properties (dielectric and electric properties, charge behavior)
	Approaches for selective powder deposition	<ul style="list-style-type: none"> • Mechanical vibration-based approaches • Electrostatic based approaches • Aerodynamic based approaches • Combined approaches
Dimensions of applicability	Dimensions of operability	<ul style="list-style-type: none"> • Process time • Resolution and precision of material selectivity • Compensation of substrate irregularities • Material flexibility • System complexity • Robustness and reliability • Powder management and powder conditioning
	Dimensions of powder layer quality	<ul style="list-style-type: none"> • Layer height • Relative density • Homogeneity • Material composition & contamination

Fig. 1 Framework for evaluating the applicability of SPD approaches for additive manufacturing technologies that utilize powder beds

desired mechanical, thermal and geometric properties of the manufactured parts [10].

2.2 Review and discussion of SPD approaches

Principles used for SPD emerge by implementing physical effects, which ideally fulfill the dimension of applicability in a technical realization. Technical implementations can be differentiated according to the type of powder deposition (direct, indirect), the effect type (mechanical, aerodynamic, electrostatic) and dimensionality (point-like, linear, and planar) of their formative elements as well as the dimensionality of their powder application elements. The type of powder application refers to process steps necessary for enabling material selectivity and deposition of the powder. If both steps are performed simultaneously, the term *direct* is assigned, otherwise *indirect*. Formative elements serve to

achieve material selectivity and are equivalent to the powder application elements in direct use. In indirect deposition, the powder pattern is created on a secondary element, which is used for the transfer to the substrate and powder bed. The SPD principles and devices discussed in the literature with respect to additive manufacturing technologies that utilize powder beds are mainly direct vibration-assisted SPD implementing nozzles [24, 27–36], indirect SPD using the electrostatic principle [37–44] and powder deposition or removal using aerodynamic approaches [25, 45–47].

Vibrating powder deposition devices (VPDD) enable direct material selectivity by controlling the flow of powder through a sub-millimeter orifice in a time-dependent manner. The inherent valve function results from the formation of powder bridges when the aspect ratio of the flow channel and grain diameter reaches a critical level. This formation can be disrupted by mechanical stimulation. Furthermore,

a correlation between mass flow and excitation intensity, which is a function of the amplitude and frequency of the mechanical vibrations, enables a controlled flow of the powders [29, 30, 32]. Two main types of actuators have been used to stimulate this process: electrodynamic [24, 48] or piezoelectric [28–32, 35, 49–53]. Both induce vibration into the formative element, along or perpendicular to the axis of gravity. The frequencies used so far range between 100 Hz [30, 48] and 50 kHz [51], with amplitudes as low as 15 μm [48] and up to 250 μm [29]. Layer thicknesses of 70 μm [24] and track widths of 85 μm [28] have been documented, which matches typical layer heights and melt pool widths in PBF-LB [54], thus demonstrating the applicability of VPDD in this respect. In addition, the application of powder tracks with a high powder layer quality at trajectory velocities of up to 13 mm/s has been demonstrated, while higher velocities pose a limit due to an increase in the void volume fraction [28, 29]. Together with the sub-millimeter track widths that determine the resolution of material selectivity, this results in increased process times when considering the VPDD dimensions commonly used in the literature. Nevertheless, the simultaneous use of formative elements arranged in a pseudo-element of higher dimensionality could, in principle, reduce the process time. However, the large size of individual formative elements currently allows only a small number to be implemented, providing limited added value. Another challenge is the application of VPDD, which requires knowledge of the correlations between influencing variables (excitation intensity, powder properties) and resulting variables (track width, powder layer quality dimensions). Powder discharge relies on driving body forces caused by excitation and gravity, which is hindered by retarding adhesive forces [55]. Although lower density materials tend to be more difficult to process, there is no general limitation on the classes of materials, which can be processed. Ultimately, the use of dry powders with sufficient flow characteristics, such as low internal friction and resistance to compaction, can result in robust and reliable powder application processes. VPDD offer advantages, particularly with their inherent ability to compensate for substrate irregularities occurring as process artifacts [56, 57] and their potential ability to produce a superior powder layer quality when applied as powder ductors.

Electrographic powder deposition devices (EPDD) utilize the electrophotographic principle [39, 40, 42] and achieve material selectivity by conditioning a photoconductor applied to a carrier electrode. Therefore, the photoconductor is electrostatically charged, ideally homogeneously, which is selectively reduced by light irradiation exploiting the photoelectric effect. Thus, the light source represents the formative element of this indirect method, which is punctually projected (e.g., when using a laser or other punctually focused light source [38]) or arranged in pseudo-elements

mimicking a one-dimensional [44] or two-dimensional [41] projection. The prepared carrier electrode is then positioned over a second electrode, which is covered by a powder layer spread on top. An electric field of approximately 10^5 – 10^6 V/m is subsequently established between the two electrodes [38, 39, 41], with the polarity of the electrodes varying depending on the approach [41]. The electrostatically charged powder particles are attracted to the carrier electrode of the photoconductor according to the charge pattern created by the previous illumination. The resulting powder pattern is ultimately applied to the substrate. For this, the carrier electrode is electrically grounded and an electric field is applied across the electrode and the substrate, causing the electrostatically charged powder still adhering to the photoconductor to move towards the substrate. The functionality of this method has been demonstrated for ceramics [44], glass [41], polymers [41, 42] and metals [37–39, 58]. However, there are material-specific challenges. When processing powders of dielectric materials, the electric field is affected by the inhomogeneous structure of the substrate. This effect is related to the height of the substrate and negatively affects powder transfer from the carrier plate to the substrate [44]. As an alternative, the application of an additional powder transfer electrode positioned between the carrier plate and the substrate has been previously investigated [41]. Configured as a wire mesh, the electrode hinders the powder transfer and negatively affects the resolution and precision of the material selectivity and the quality of the powder layer [41]. Regardless of the class of material processed, there are further challenges requiring additional investigations. For example, a single powder transfer step may not achieve adequate coverage of the areas to be coated [38, 39, 41, 42]. As an example, Förster et al. [39] demonstrated complete coverage after twenty repetitions using metallic powders. This effort scales with the number of processed powders and increases the overall process time as a consequence. In addition, a residue-free transfer of powder is not possible, therefore, a regular and thorough cleaning of the photoconductor is currently unavoidable. In the case of metallic powders, a resolution of material selectivity in the range of 5 mm has been demonstrated [38]. In summary, the operability of EPDD systems currently is limited by increased process times, the absence of abilities to compensate for substrate irregularities, the overall system complexity and a resolution of material selectivity, which is an order of magnitude greater than the typical scale of melt pools. Moreover, the quality of the powder layer for dielectric materials is limited, which currently results in a restricted applicability.

Aerodynamic powder deposition devices (APDD) proposed in the literature generate selective powder beds both directly [45] and indirectly [25, 45–47] by deposition or removal methods using punctual formative elements of varying numbers. Technical implementations range from

suction nozzles, which remove powder from an already deposited layer on the substrate [25, 46] to more sophisticated approaches implementing an array of micro-nozzles to assemble pseudo-formative elements [45]. When using suction nozzles, contamination can occur in the form of residual particles from incomplete removal [25, 46]. In addition, contamination of the removed powder volume occurring during removal requires further efforts to separate the powder types [25]. More sophisticated system configurations are presented in a patent by Bederot et al. [45]. They suggest using a complex system of micro-nozzles, which control gas flows in combination with a thin film screen allowing gas flows but not processable powder particles to pass through. Both direct and indirect approaches are discussed, each offering a theoretical selectivity resolution of 100 μm based on the nozzle arrangement. In both methods, the processed powder is first homogeneously spread on the screen. In the case of indirect application, excess powder on the screen is selectively ejected by activating the respective microvalves. This process results in a powder pattern on the screen, which is applied to the substrate as the next layer through an ejection element. In this case, the screen acts as a planar powder application element. In the direct approach, the screen merely acts as a powder feeder from which the powder is selectively ejected and transferred directly to the substrate through micro-nozzles, which compose a formative pseudo-element. Both the indirect and direct methods facilitate low process times but require complex systems. Since these processes involve raking operations for coating the screens, the flow properties of the processed powders are relevant and may determine the requirements regarding the powder condition. While there is no fundamental limitation on the material classes possibly processed, there is a lack of experimental results in the literature on the achievable powder layer qualities. However, conclusions can be drawn from the principles of the process for a preliminary assessment. Initially, it is reasonable to assume, a reliable process, provided the powder is conditioned as required, the valves are designed for safe operation, no particles are jammed in the screen and process parameters are set correctly. Under these conditions, the process is likely to have a low susceptibility to contamination, but powder layers may lack homogeneity and exhibit increased void volume fractions. Considering the homogeneity of the applied powder layer, there are additional risks regarding a possibly incomplete transfer, which could be caused by flow disturbances with the screen itself. Concluding, APDD is capable of achieving conventionally used layer heights and a high level of selectivity while maintaining process times comparable to conventional powder applications in mono-material processing. However, APDD lacks the ability to compensate for substrate irregularities, e.g., by selectively adjusting the deposited thickness and may lead to an inferior quality of the powder layers.

Conclusion of the State of the Art and Potentials for Research and Development The analysis of the current state of the art suggests that the powder layer quality achievable with VPDD surpasses the powder layer qualities achieved with EPDD and APDD. Despite this advantage, VPDD also exhibits relevant shortcomings regarding its operability. These deficits are results of low deposition rates and a lack of understanding of the relationships between influencing variables and resulting quantities. Currently, the literature does not provide any equation-based correlations to address this knowledge gap. To mitigate this gap, an application method for VPDD is proposed in the following chapters. For this purpose, a preliminary study of typical control and resulting quantities is performed using DEM on basis of virtual simulations. The results are summarized and derived in this study as the dimensionless quantities Π and used to describe the flow behavior of the investigated powders. In addition, these relationships are validated through physical experiments, which is achieved with a novel miniature VPDD developed based on the simulation results. The compact size of the device, with a diameter of 11 mm, facilitates the assembly of formative pseudo-elements and enables the mitigation of a major shortcoming of the VPDD, which is the low deposition rate. Consequently, this research effort could significantly enhance the operability of VPDD and pave the way for its improved applicability.

3 Materials and methods

In order to investigate technological potentials as well as explore and enable the necessary boundary conditions for a prototypical implementation of VPDD, a methodological approach (Fig. 2) is presented, which includes virtualized experiments (denoted by the index *sim*) as well as validation experiments in a real physical setup (denoted by the index *real*). Compared to physical approaches, analyses based on virtual process models avoid the introduction of confounding influences, since these can be excluded during modeling. Moreover, input variables can be precisely defined independent of each other and the state and process variables associated with powders used in additive manufacturing are more easily accessible through virtual approaches as well. DEM is used to investigate the influence of harmonic oscillations (frequencies up to 1500 Hz and amplitudes up to 45 μm) on the quality of selectively deposited powder tracks in virtual environment (Fig. 2, steps I–IV). This is accomplished using dimensionless quantities Π derived in this research, which correlate resulting parameters (powder layer quality) with influencing input variables (such as deflection vectors of three different orientations, geometric parameters and flow

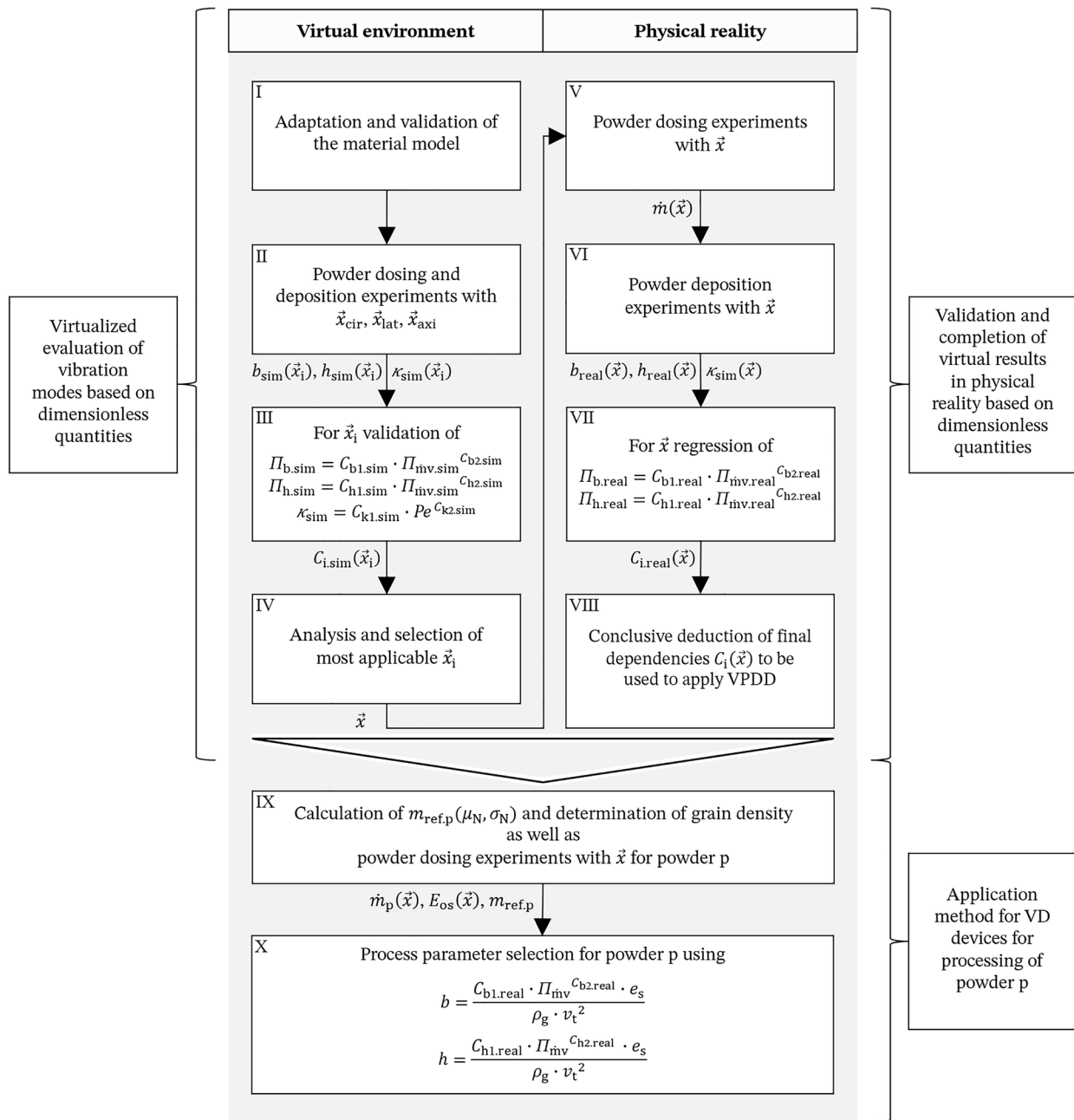


Fig. 2 Methodology for a generic approach to the process parameter selection based on dimensionless quantities, expressing relationships between influencing variables and resulting quantities

properties of powders). In addition, the identified most suitable deflection vector orientation is investigated with experiments using a novel VPDD prototype (Fig. 2, steps V–VIII). The results are summarized in an application method for VPDD, which is based on the dimensionless quantities (Fig. 2, steps IX–X). The materials and virtual as well as physical methods used in this research are detailed in the following sections.

3.1 Characterization of investigated powders

In order to explore the versatility of the method across different classes of materials encountered in PBF, this research includes investigations on AlSi10Mg (AlSi10Mg.02, m4p material solutions, Germany), Al (PureAl.01, m4p material solutions, Germany), Al₂O₃ (BAK40; distributor: xtra, Germany) and polyether ether ketone (PEEK; Vestakeep 2000 FP, Evonik, Germany). Within this group of examined

powders, data from the virtual investigation of deflection vector orientations and its influence on powder layer quality is only obtained for AlSi10Mg. In order to provide a relative comparison between the studied powders, their flow properties must be considered, which are mainly determined by the interactions of effective surface and body forces acting on the particles and can be considered based on particle density and morphology. In this study, the qualitative morphology description consists of the sphericity and roundness of the particles in conjunction with the particle size distributions (PSD) of the bulk, which can be expressed by its corresponding distribution values. While sphericity and roundness determine the rolling resistance of the particles, the PSD is relevant, as it affects the ratio of surface to body forces [59]. Roundness is characterized as the ratio of the average radii of convex regions of a particle to the radius of its circumscribing circle. Similarly, the circularity of a particle denotes the ratio of the circumference of a circle of equal area to the actual circumference of the particle. Both of these metrics refer to two-dimensional projections. The evaluation of grain shape is based on SEM images (Fig. 3, analyzed with a Supra 55VP Gemini, Carl Zeiss, Germany).

Compared to Al₂O₃ powder, both AlSi10Mg and Al powders exhibit lower roundness values due to the presence of bonded satellites and a reduced circularity as a result of partial elongation. The PEEK powder, characterized by its polygonal shape, has the lowest sphericity and roundness among the powders investigated. Gravimetric sieve analyses according to ISO 4497:2020-10 [60] are performed to determine the particle size distributions (balance PNJ 600-3 M, Kern & Sohn, Germany). Investigations are carried out using test sieves according to ISO 3310-1 with mesh sizes of 20/25/32/38/45/50/56/63/71/80 μm (Haver & Böcker, Germany) mounted on a sieve shaker (AS 200 basic, Retsch, Germany). The obtained mass fractions are initially approximated through a log-normal distribution [59]. By assuming a spherical grain shape, the mass-specific distribution

is then transformed into a grain number-based distribution. The transformation takes place within the density function at points i using the proportionality of mass and volume, and the relative scaling of the sphere volume over the grain radii:

$$\varphi_{mi} \cdot r_0^3 / r_i^3 = \varphi_{Ni} \quad (1)$$

Here, φ_{mi} refers to the value of the mass-specific density function at a location i , r_0 signifies the reference grain radius and r_i denotes the grain radius. The determined mean of the log-transformed values, μ_N , and corresponding standard deviations, σ_N , are presented in Table 1 for distributions based on both mass and number of grains.

3.2 Simulative setup

The powder deposition simulations are performed using EDEM software (Altair Engineering Inc., Troy-USA). The contact model consists of several sub-models, including Hertz [61] and Mindlin [62] normal and tangential forces. Damping forces in corresponding directions as proposed by Tsuji et al. [63], an adhesive force element derived from Johnson et al. [64] and a standard rolling friction model, are also implemented. The selection of the contact model as well as its parameterization are based on previous research

Table 1 Determined distribution values of grain diameter d [μm] for AlSi10Mg powder, Al powder, Al₂O₃ powder, and PEEK powder

Powder materials	Mass-specific size distribution		Number-specific size distribution	
	$\mu_m[-]$	$\sigma_m[-]$	$\mu_N[-]$	$\sigma_N[-]$
AlSi10Mg	3.56	0.228	3.52	0.204
Al	3.60	0.326	3.42	0.291
Al ₂ O ₃	3.85	0.243	3.76	0.217
PEEK	3.95	0.203	3.89	0.181

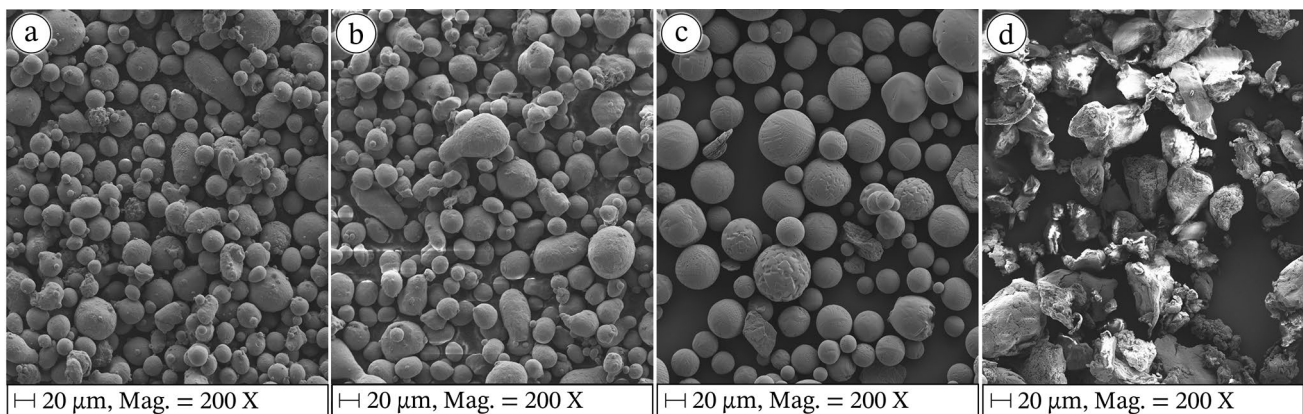


Fig. 3 Virtual SEM micrographs of the investigated powders: **a** AlSi10Mg **b** Al **c** Al₂O₃ and **d** PEEK powder

by the authors [59] for monospherical particles, which also includes a detailed presentation of the governing mathematical models used. Parameters not included there for the particle–VPDD contact were determined with respect to the coefficients of sliding friction and restitution as described in Ref. [59] using inclination and rebound experiments. The rolling friction coefficient in the particle–VPDD contact is set to half of the value for the particle–particle contact to account for the flat silanized surface of the VPDD, which provides lower rolling resistance compared to the irregular surfaces of individual particles. By emulating the missing effects resulting from the lack of a geometrically modeled surface roughness of the substrate, the parameters describing the contact between substrate and particles were manually adjusted (Table 2) to improve the simulation results.

The simulation model consists of a substrate plate and a tubular VPDD (with an inner diameter of $D_1 = 500 \mu\text{m}$ and an outer diameter of $D_2 = 1000 \mu\text{m}$) filled with 200,000 particles (Fig. 4). Starting from the right ($x_{i=0} = -D_1/2$), the dispenser is moved uniformly over the substrate for

a distance of $5000 \mu\text{m}$ while maintaining the distance h_0 and the velocity v_t . In addition, deflection vectors $\vec{x}_i(t)$ are imposed on the device, which can be described as follows:

$$\vec{x}_{\text{lat}}(t) = \hat{x} \cdot [\sin(\omega \cdot t) \ 0 \ 0]^T, \quad (2)$$

$$\vec{x}_{\text{axi}}(t) = \hat{x} \cdot [0 \ 0 \ \sin(\omega \cdot t)]^T, \quad (3)$$

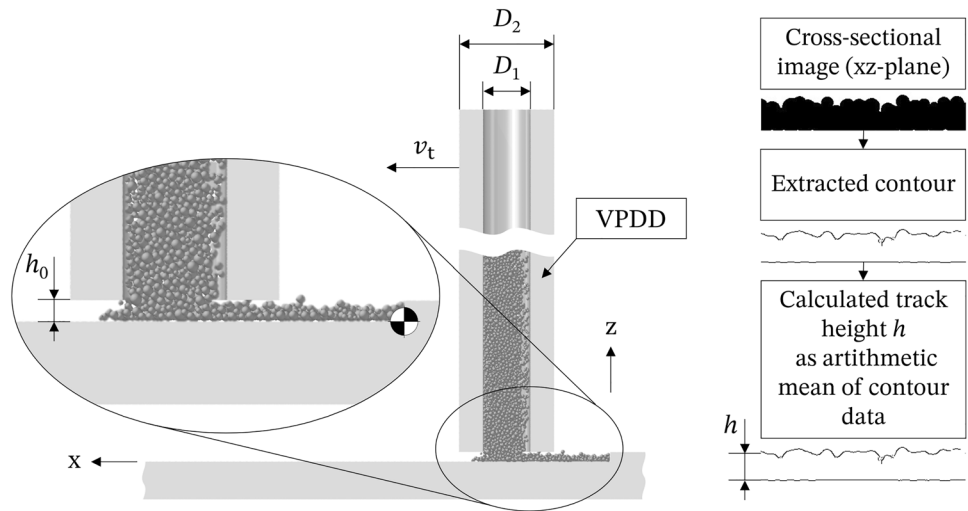
$$\vec{x}_{\text{cir}}(t) = \hat{x} \cdot [\sin(\omega \cdot t) \ \cos(\omega \cdot t) \ 0]^T. \quad (4)$$

The orientations of the x-, y-, and z-directions refer to those given in Fig. 4. In accordance with Eqs. 2–4, the following analysis does not explore the potential influence of an angular relationship between the direction of translation and the direction of vibration amplitude during uniaxial vibration. However, alternating the relative orientation of v_t affects the perpendicular components of $\vec{x}_{\text{lat}}(t)$, while $\vec{x}_{\text{cir}}(t)$ exhibits only a phase shift and is, therefore, considered less

Table 2 Parameters used for the DEM simulations; both model parameters determined for AISi10Mg powder and process parameters

Parameters	Symbols	Units	Values and value ranges
General parameters [59]			
Young's modulus	E_{sim}	Pa	75×10^6 (equals 0,1% of E_{real})
Poisson's ratio	ν	[-]	0,33
Surface energy density	w_{JKR}	J/m ²	2.25×10^{-3}
Solid density of a particle	ρ_g	kg/m ³	2670
Surface of a reference particle	A_{refN}	m ²	3.72×10^{-9}
Mass of a reference particle	m_{ref}	kg	3.43×10^{-11}
Mean value of d [μm] (log-normal, N-spec.)	μ_N	[-]	3.56
Standard deviation of d_p [μm] (log-normal, N-spec.)	σ_N	[-]	0.228
Lower capping value ($\varphi_{N_i} \leq 3.5\%$)	c_{low}	μm	20
Upper capping value ($\varphi_{N_i} \leq 0.35\%$)	c_{high}	μm	60
Time step	T_{sim}	s	1.34×10^{-7}
Parameters of particle to particle contact [59]			
Coefficient of sliding friction	$\mu_{s \text{ pp}}$	[-]	0.2
Coefficient of rolling friction	$\mu_{r \text{ pp}}$	[-]	0.0808
Coefficient of restitution	$c_{\text{res pp}}$	[-]	0.54
Parameters of VPDD wall to particle contact			
Coefficient of sliding friction	$\mu_{s \text{ dp}}$	[-]	0.1
Coefficient of rolling friction	$\mu_{r \text{ dp}}$	[-]	0.04
Coefficient of restitution	$c_{\text{res dp}}$	[-]	0.52
Parameters of substrate to particle contact			
Coefficient of sliding friction	$\mu_{s \text{ sp}}$	[-]	0.8
Coefficient of rolling friction	$\mu_{r \text{ sp}}$	[-]	0.6
Coefficient of restitution	$c_{\text{res sp}}$	[-]	0.54 [59]
Process parameters			
Translational velocity of the dispenser	v_t	mm/s	25, 50, 75, 100
Frequency of oscillation of the dispenser	f	1/s	500, 1000, 1500
Amplitude of oscillation of the dispenser	\hat{x}	μm	10, 20, 30
Distance between substrate and dispenser tip	h_0	μm	100, 200

Fig. 4 Virtual setup and corresponding geometric parameters such as the height of the annular gap between the substrate and the tube tip h_0 , the inner and outer diameters D_1 and D_2 as well as an example of the image-based evaluation of the track height (width is evaluated analogously)



sensitive. The evaluation of the powder track condition is performed both directly in EDEM and by image-based contour extraction (approximately 1000 measurement points per contour) based on arithmetic means. Track height is assessed in cross-sectional images within the xz -plane, centered on the powder track, while track width is determined from top-view images. In EDEM, the void volume fraction κ of the applied powder track is calculated from the arithmetic mean of 10 grid bins as follows:

$$\kappa_{\text{sim}} = 1/10 \cdot \sum_{i=0}^{10} (1 - V_{p,i}/V_{c,i}), \quad (5)$$

where $V_{p,i}$ refers to the powder volume located within the i -th control volume $V_{c,i}$. The control volumes are arranged along the powder track in the xy plane and are mirror-symmetrically positioned with respect to the xz -plane, with dimensions of 500 μm , 300 μm , and 50 μm in the x -, y -, and z -directions, respectively.

3.3 Physical setup

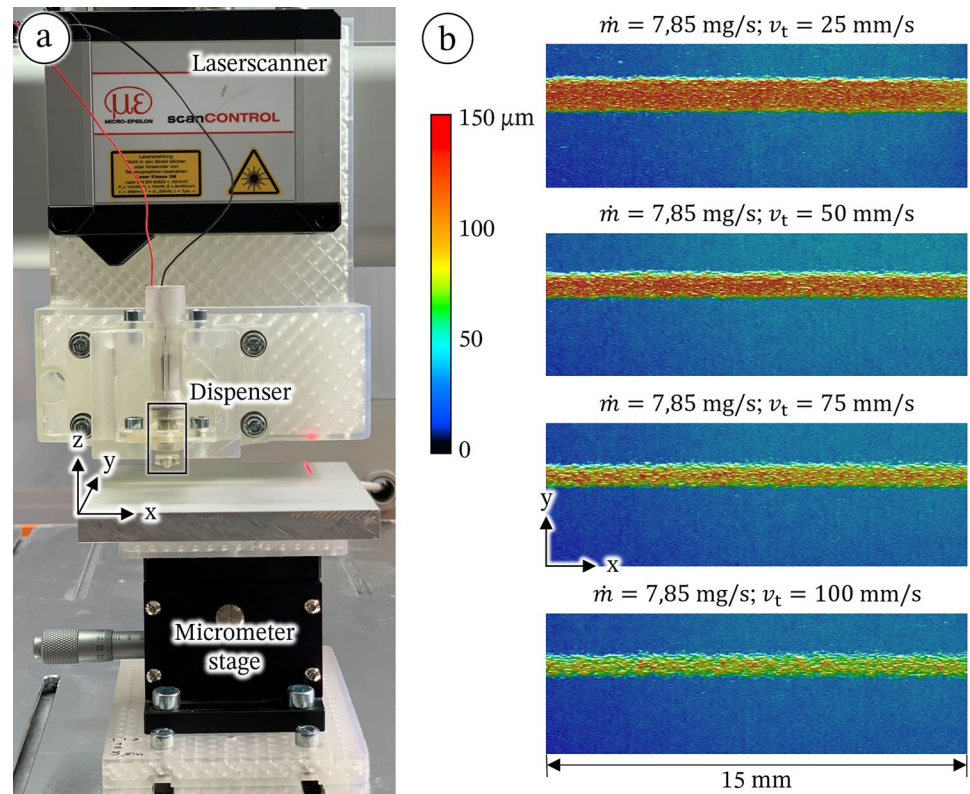
The validation experiments in a physical setup are conducted with oven-dried powders with a moisture content of less than 0.05% by mass (measured with a DAB 100-3 moisture analyzer, manufactured by Kern & Sohn GmbH, Balingen-Germany), and a novel miniaturized VPDD, designed according to the results of the DEM studies and discussed in more detail in Sect. 5.2. The goal of the experimental series is to correlate VPDD control variables, such as the deflection vector, with mass flows and resulting powder layer quality based on powder deposition tests. The deflection vector is measured uniaxially near the outlet using a laser vibrometer (projection dimension: point; model: optoNCDT ILD2300-10, manufactured by Micro-Epsilon Messtechnik GmbH & Co. KG, Ortenburg-Germany). For mass flow measurements,

the dispenser is positioned 30 mm above the weighing pan of an analytical balance (model: PNJ 600-3M; manufacturer: Kern & Sohn GmbH, Balingen-Germany), which ensures free flow of the powder during measurements. For powder deposition experiments, the VPDD is uniformly translated over an AlSi10Mg substrate plate using a CNC portal setup (Fig. 5a). For an optimized alignment, the substrate plate is leveled by planar milling in the same CNC portal and is glass bead blasted afterwards ($R_z = 69.7 \mu\text{m}$; measured with a confocal Laser Scanning Microscope or LSM, on a square area of 500 μm side length; LSM model: VK-X160K, manufactured by Keyence, Osaka-Japan). Leveling in the z -direction is achieved using a micrometer stage. Measurement of the powder track is carried out using a laser distance meter (projection dimension: line; model: scanCONTROL 3060-25, manufactured by Micro-Epsilon Messtechnik GmbH & Co. KG, Ortenburg-Germany). The width and height of the powder track are determined over sections with a length of 15 mm (Fig. 5b), which are divided into 400 profiles based on the maximum values of each profile.

4 Derivation of the dimensionless quantities

Dimensionless quantities, which are based on Buckingham's Pi theorem [65], i.e., the assumption that physical relationships hold independently of the units used to measure the dimensions of length, mass, time and temperature, are used in various areas of science as they can promote and simplify the understanding and description of complex physical phenomena. This is achieved through a systematic dimensional analysis and reduction of the included input variables to a few dimensionless quantities. In the field of additive manufacturing technologies that utilize powder beds, dimensionless quantities are applied primarily

Fig. 5 **a** Setup for physical experiments, **b** measured powder tracks in top view with color-coded powder track height



for thermal and rheological modeling. The former aims to improve the comprehension of the dominant heat transfer mechanisms and their associated mechanisms. In this context, dimensionless quantities such as the Péclet number have been used to predict convection, as well as conduction mechanisms and their relative impacts on the process [66–68]. Rheological modeling, on the other hand, is useful for emulating powder dynamics processes described by dimensionless quantities such as the bond number [14, 69] or a specialized type of the Péclet number, which relates the characteristic deformation and relaxation times in a sheared powder volume [14, 69, 70]. These parameters facilitate the quantification and comparison of the relative importance of inertia and gravity effects. The use of dimensionless quantities enables effective comparisons of processes conducted at different scales and under varied conditions. Furthermore, they also allow a physical interpretation of processes and phenomena at a reduced level of complexity. However, their utility is not without disadvantages, as they often depend on assumptions, which condition their practical applicability regarding the correct modeling of the prevalent physical effects. For example, idealizing flow conditions or ignoring certain heat transfer mechanisms may not be valid in reality and could decrease the quality of prediction. In addition, dimensionless quantities can lead to erroneous predictions when applied outside the scope for which they were derived. Concluding,

the proper use and interpretation of these dimensionless quantities requires a thorough understanding of the underlying physical principles and mechanisms.

To employ dimensionless quantities to facilitate the application of VPDD, the first step is to identify, which variables should be correlated. In terms of resulting quantities, dimensions related to powder bed quality such as layer height h , void volume fraction κ , homogeneity ξ and the width b of the applied powder tracks are significant. Regarding the influencing variables, the derivation of the dimensionless quantities can be based on powder flow properties (influenced by morphology, grain density and moisture content), the mechanical energy input for powder fluidization (described by the vibration parameters), the geometrical conditions and the translational velocity of the dispenser v_t . However, considering the significant experimental efforts necessary for a comprehensive determination of powder properties, it is advantageous to condense them into resulting quantities. In order to reduce the number of parameters, both groups are combined into excitation specific mass flow functions $\dot{m}(E_{os}, A_1)$ and are included in the formulation of dimensionless quantities together with the easily accessible grain density ρ_g . The mass flow functions are based on the area of the circular orifice of the nozzle A_1 , as well as the energy of the oscillation E_{os} and determined during the free discharge. Therefore, the mathematical relationship is

$$A_1 = \pi \cdot (D_1/2)^2, \tag{6}$$

$$E_{os} = \hat{E}_{kin}, \tag{7}$$

$$\hat{E}_{kin} = \frac{1}{2} \cdot m_{ref} \cdot (\hat{x} \cdot \omega)^2. \tag{8}$$

Here, D_1 is the orifice diameter of the nozzle, \hat{x} is the amplitude of vibration, ω is the angular frequency of vibration, and m_{ref} is the reference grain mass according to

$$m_{ref} = \sum_{i=c_{low}}^{c_{high}} (\varphi_{Ni} \cdot m_{Ni}) / \sum_{i=c_{low}}^{c_{high}} \varphi_{Ni}, \tag{9}$$

where φ_{Ni} is the value of the density function of the number-based grain size distribution at location i . The indexing of m_{Ni} is analogous. In addition to the nozzle orifice area, the geometric quantity determining the powder outflow is the reference shell area A_s of the annular gap between the nozzle tip and the substrate

$$A_s = \pi \cdot D_{ref} \cdot h_0. \tag{10}$$

Here, D_{ref} is a reference radius (here 1000 μm) and h_0 is the distance between the nozzle tip and the substrate. The drive of the powder to propagate through the annular gap is modeled based on the characteristic energy density e_s in the sheared cross-section following

$$e_s = E_{os}/A_s. \tag{11}$$

According to this simplified view, the general correlation is given by

$$b, h, \kappa, \xi = f(h_0, D_1, A_s, \rho_g, v_t, \dot{m}(E_{os}, A_1), e_s). \tag{12}$$

The derivation of dimensionless quantities by dimensional analysis (Table 3) is performed for the powder track width and the excitation specific mass flows as non-repeating variables. For the application, ρ_g and the control

variables v_t and e_s are used as repeating parameters along with the nozzle geometry $D_1, A_s = \text{constant}$. Void volume fraction and homogeneity are not considered at this stage and are primarily used to evaluate the powder layer quality under different combinations of the other input variables within a simulation environment.

The dimensionless parameters, therefore, follow as

$$\Pi_{\dot{m}} = \rho_g \cdot v_t^3 \cdot e_s^{-2} \cdot \dot{m}, \tag{13}$$

$$\Pi_b = \rho_g \cdot v_t^2 / e_s \cdot b. \tag{14}$$

Equation 13 describes a velocity ratio according to

$$\Pi_{\dot{m}} = (v_t/v_{dif})^3, \tag{15}$$

which is influenced by the excitation-dependent achievable diffusion velocity of the powder flow v_{dif} . Equation 14 can be interpreted as the time quotient of the diffusion and advection time by expanding it according to the square of the track width b . Thus, Π_b describes the ratio between the time required for a representative particle to move a given distance by diffusion and the time it would take to move the same distance by advection, in terms of the trajectory velocity. Therefore, it follows

$$\Pi_b = (t_{dif,b}/t_{adv,b})^2, \tag{16}$$

$$t_{dif,b} = (b^3 \cdot \rho_g / e_s)^{0.5}, \tag{17}$$

$$t_{adv,b} = b/v_t. \tag{18}$$

As the dimensions are equal, it is possible to consider the resulting layer thickness instead of the track width as well. Therefore,

$$\Pi_h = \rho_g \cdot v_t^2 / e_s \cdot h \tag{19}$$

applies. The quotient

Table 3 Systems of equations of dimensional analysis for (a) $\Pi_{\dot{m}}$ with the nonrepeating variable \dot{m} and (b) Π_b with the nonrepeating variable b

(a)	Dimensions	ρ_g	v_t	e_s	$\dot{m}(E_{os}, A_1)$
	Mass	1	0	1	1
	Length	-3	1	0	0
	Time	0	-1	-2	-1
(b)	Dimensions	ρ_g	v_t	e_s	b
	Mass	1	0	1	0
	Length	-3	1	0	1
	Time	0	-1	-2	0

$$\Pi_{\dot{m}}/\Pi_b = (v_t/v_{\text{dif}})^3 / (t_{\text{dif},b}/t_{\text{adv},b})^2 \quad (20)$$

indicates how much advection dominates over diffusion during powder deposition and can, therefore, be interpreted as the Péclet number Pe . A Péclet number below one indicates that diffusion dominates over convection, for Pe bigger than one, the opposite is true. It can, therefore, be generally concluded, that the lower the Pe , the lower the risk of advective powder entrainment leading to diffusive accumulation of powder around the outlet, favoring a reduction in void volume fraction.

For this reason, the Péclet number formulated here is used as a characteristic quantity for assessing the resulting void volume fraction.

5 Results and discussion

In this chapter, the experimental results are presented and analyzed to facilitate the application of VPDD by investigating the validity of the approach presented in Sect. 3 (Fig. 2). First, the effects of differently oriented vibrational deflections are investigated using the example of a capillary tube to dispense powder (Fig. 4 in Sect. 3.2). The results are analyzed based on the dimensionless quantities derived in Chapter 4 and additionally compared regarding the resulting powder bed quality. As a result, the most suitable approach is implemented in a novel miniature VPDD, which is introduced and used for validation in physical reality.

5.1 Simulative investigation on deflection vectors

The influence of the deflection vector on the quality of the applied powder tracks is investigated as a preliminary evaluation for later implementation of the results in a physical device. Simulations are performed with DEM under the conditions specified in Sect. 3.2 for AlSi10Mg powder, assuming a monospherical grain shape. The investigated parameter combinations are divided into four series of constant translation velocities, in which identical combinations of oscillation frequency and amplitude are studied. Analysis of the simulation results is based on the dimensionless quantities $\Pi_{\dot{m}}$, Π_b and Pe derived in Chapter 4. When originally plotted in this system, the results for $\Pi_b(\Pi_{\dot{m}})$ and $\Pi_h(\Pi_{\dot{m}})$ show small coincidence errors in the curve progressions. These are assumed to be a result of the inhibition of powder outflow from the nozzle orifice due to powder located in the annular gap. Based on this assumption, it is concluded that low convection times at higher translation velocities entail a thinly populated annular gap and thus a higher efficiency of $\dot{m}(E_{os}, A_1)$. This, in turn, would affect the process performance and the resulting layer properties, highlighting the

importance of fine-tuning these parameters for optimized process results. Based on this hypothesis, an improved colinearity is obtained using

$$\dot{m}_v = \dot{m} \cdot v_{\text{rel}}^{-1/4} \quad (21)$$

Here,

$$v_{\text{rel}} = v_{\text{ref}}/v_{t,i} \quad (22)$$

is the translation velocity ratio, where the reference value v_{ref} corresponds to the highest translation velocity of the test series. Particularly, the curve progressions indicate a decrease in the time ratios Π_b and Π_h with increasing mass flows when the translation velocity is kept constant (Fig. 6a, b), a behavior that can be rationalized by a decrease in the diffusion times. This behavior is facilitated by an observed proportionality between \dot{m} and E_{os} as well as the resulting correlation between E_{os} and \hat{x}^2 , f^2 (Eq. 8). Accordingly, the velocity ratio decreases with increasing diffusion velocity. For identical mass flows and increasing translation velocities, shorter advection times occur. These entail larger time ratios and velocity ratios, which is reflected in the simulation results. Thus, a relationship between volume flow and time ratios can be formulated, which is confirmed by simulations independent of the directions of the deflection vector (Fig. 7a, b). It applies

$$\Pi_{b,\text{sim}} = C_{b1,\text{sim}} \cdot \Pi_{\dot{m}v,\text{sim}}^{C_{b2,\text{sim}}} \quad (23)$$

$$\Pi_{h,\text{sim}} = C_{h1,\text{sim}} \cdot \Pi_{\dot{m}v,\text{sim}}^{C_{h2,\text{sim}}} \quad (24)$$

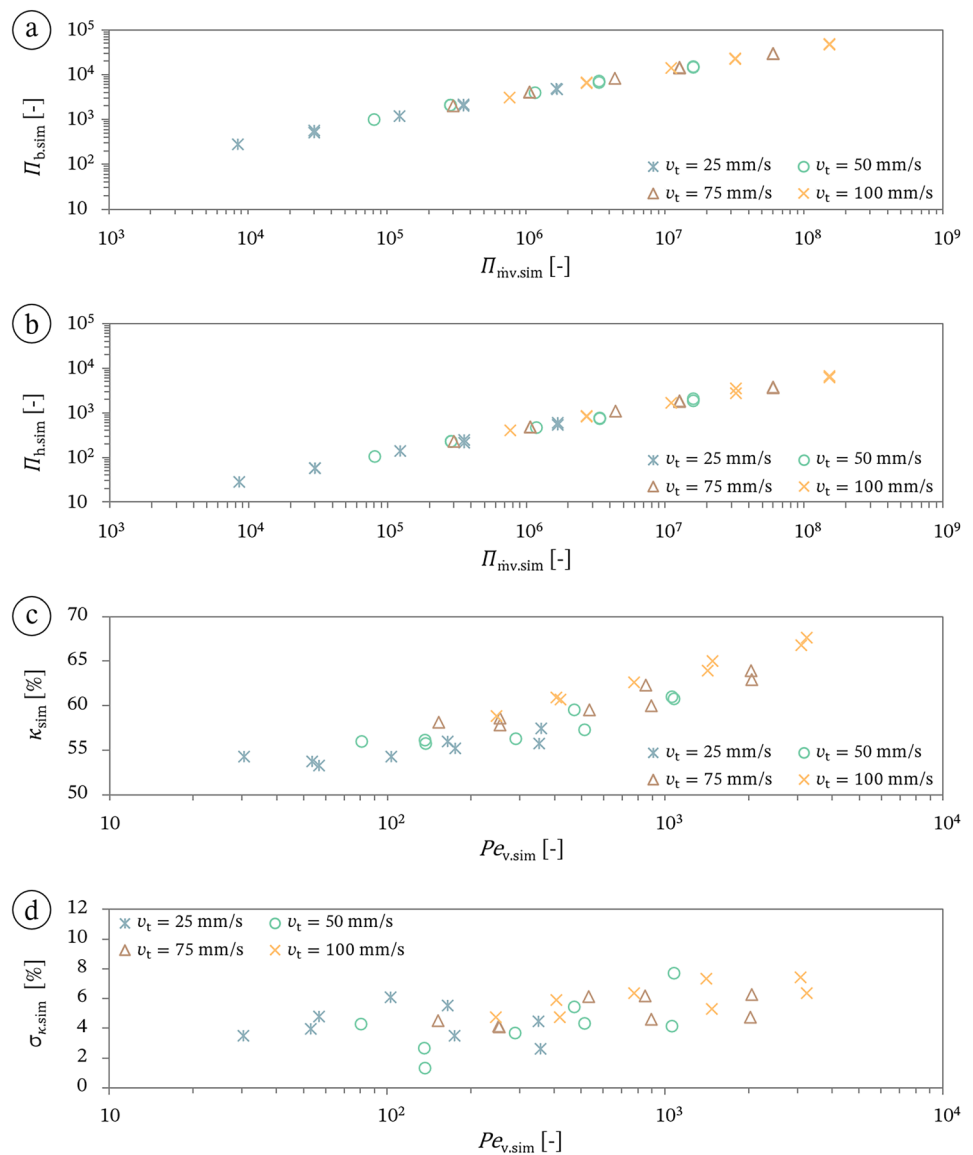
with quantities used in the virtual environment. Here, C_i are regression coefficients obtained from the analysis of experimental data (see Fig. 7). For the void volume fraction, a dependence on the translational velocity (Fig. 6c, d) as well as the directions of the deflection vectors (Fig. 7c, d) is evident. In the case of circular and lateral oscillations, regression functions can be derived, which allow an acceptable approximation of the porosities based on the Péclet number Pe_{sim} (Eq. 20). This results in the equations

$$\kappa_{\text{cir},\text{sim}} = C_{k1,\text{cir},\text{sim}} \cdot Pe_{v,\text{sim}}^{C_{k2,\text{cir},\text{sim}}} \quad (25)$$

$$\kappa_{\text{lat},\text{sim}} = C_{k1,\text{lat},\text{sim}} \cdot Pe_{v,\text{sim}}^{C_{k2,\text{lat},\text{sim}}} \quad (26)$$

The assessment of homogeneity ξ is based on the extended standard deviation of the void volume fraction σ_{κ} . The scattered void volume fractions for higher levels of axial oscillation (about $58\% < \kappa_{\text{sim}} < 76\%$) are followed by void volume fractions in lateral oscillation (about $53\% < \kappa_{\text{sim}} < 74\%$) and circular oscillation (about $53\% < \kappa_{\text{sim}} < 68\%$).

Fig. 6 Simulation results at $h_0 = 100 \mu\text{m}$ and circular oscillation for **a** powder track width $b_{\text{sim}} \approx 380\text{--}725 \mu\text{m}$, **b** powder track height $h_{\text{sim}} \approx 50\text{--}77 \mu\text{m}$, **c** cavity volume fraction $\kappa_{\text{sim}} = 53\text{--}68\%$ and **d** its calculated standard deviation $\sigma_{\kappa_{\text{sim}}} 1\text{--}8\%$



Regarding the homogeneity, the axial oscillation shows the largest deviations (about $3\% < \sigma_{\kappa_{\text{sim}}} < 11\%$), which increase with decreasing Péclet number. At lower levels, lateral oscillation (about $3\% < \sigma_{\kappa_{\text{sim}}} < 10\%$) and circular oscillation (about $1\% < \sigma_{\kappa_{\text{sim}}} < 8\%$) follow with an inverse relationship to Péclet number. Accordingly, powder application by circular oscillation produces the highest powder layer quality in the investigated area and is, therefore, transferred to physical experiments for further validation.

5.2 Miniature vibrating powder deposition device

The objective in designing VPDD is the ability to meet the required layer quality and operation boundary conditions for a potential future industrial application. According to the current state of the art, VPDDs lack operability

because they increase process times, especially due to their size-dependent limitations for sequential use. Parallelization can mitigate this disadvantage, but requires a significant reduction of the dimensions of each formative element. In addition, the deflection mode identified as most appropriate in the simulation should be used. A possible approach is the implementation of an eccentrically rotating mass (ERM) for excitation within a spring arrangement of defined stiffness, which allows a constructive match between excitation force $\vec{F}_{\text{cir}}(t)$ and deflection $\vec{x}_{\text{cir}}(t)$ of the excited structure. Realized as a function-integrated stereolithography component with an integrated ERM motor, these functions can be accommodated in a small space (Fig. 8a). The complexity of the system is low in terms of control variables, since mass flow control can be achieved

Fig. 7 Simulation results for various vibration modes and $h_0 = 100 \mu\text{m}$ for **a** powder track width $b_{\text{sim}} \approx 320\text{--}810 \mu\text{m}$, **b** powder track height $h_{\text{sim}} \approx 36\text{--}77 \mu\text{m}$, **c** cavity volume fraction $\kappa_{\text{sim}} = 53\text{--}76\%$ and **d** its standard deviation $\sigma_{\kappa,\text{sim}} = 1\text{--}11\%$

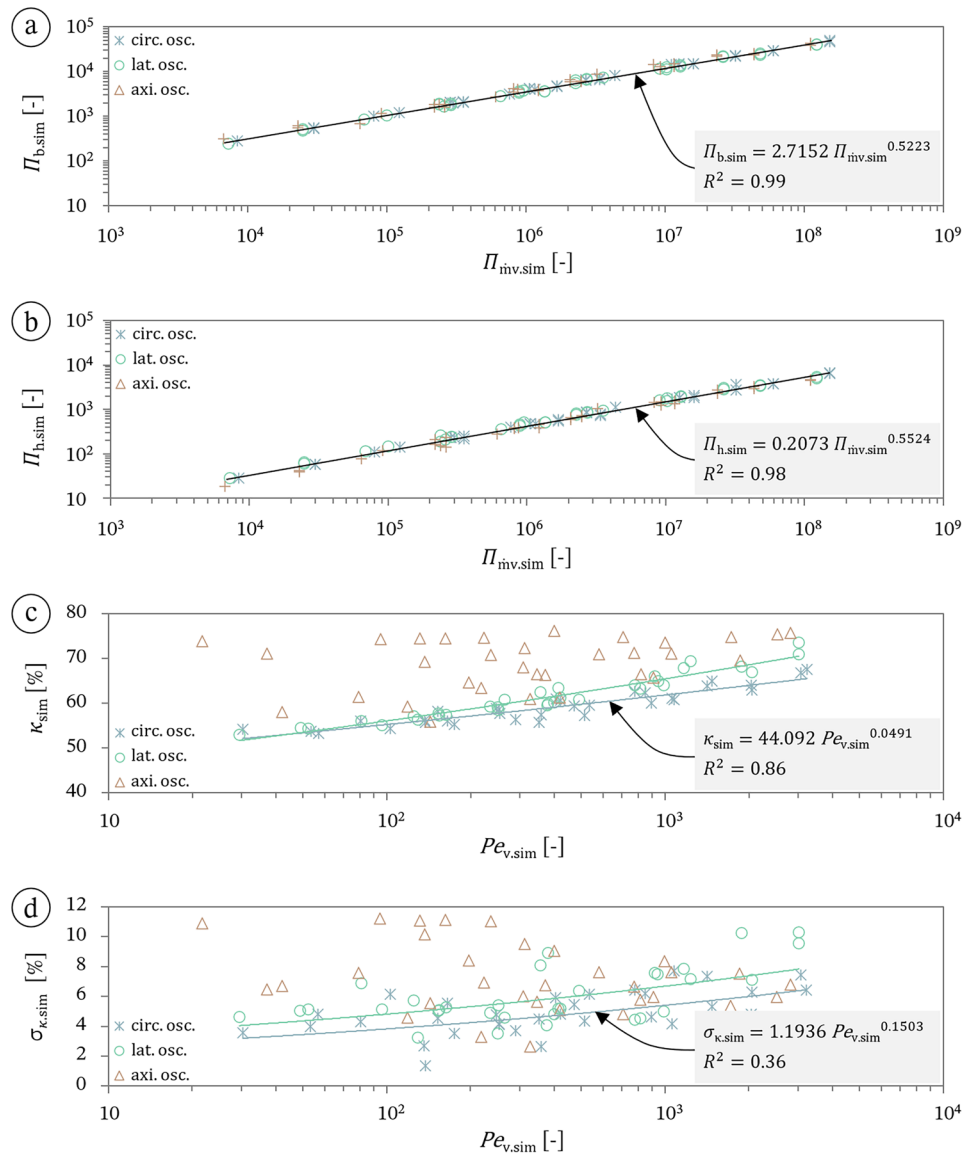


Fig. 8 a CAD drawing of the miniature VPDD used in physical experiments and **b** LSM micrograph of the dispenser outlet showing wear after processing of Al_2O_3 powder for about 4 h

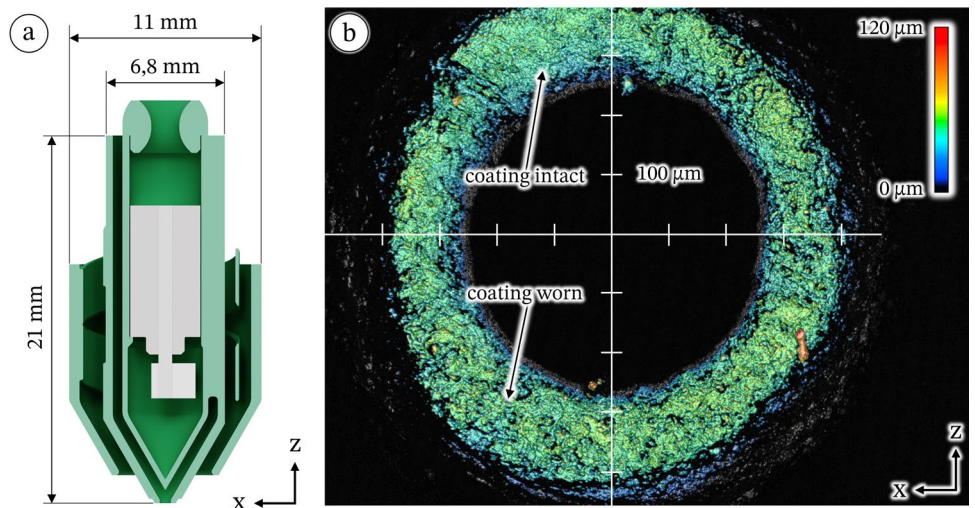
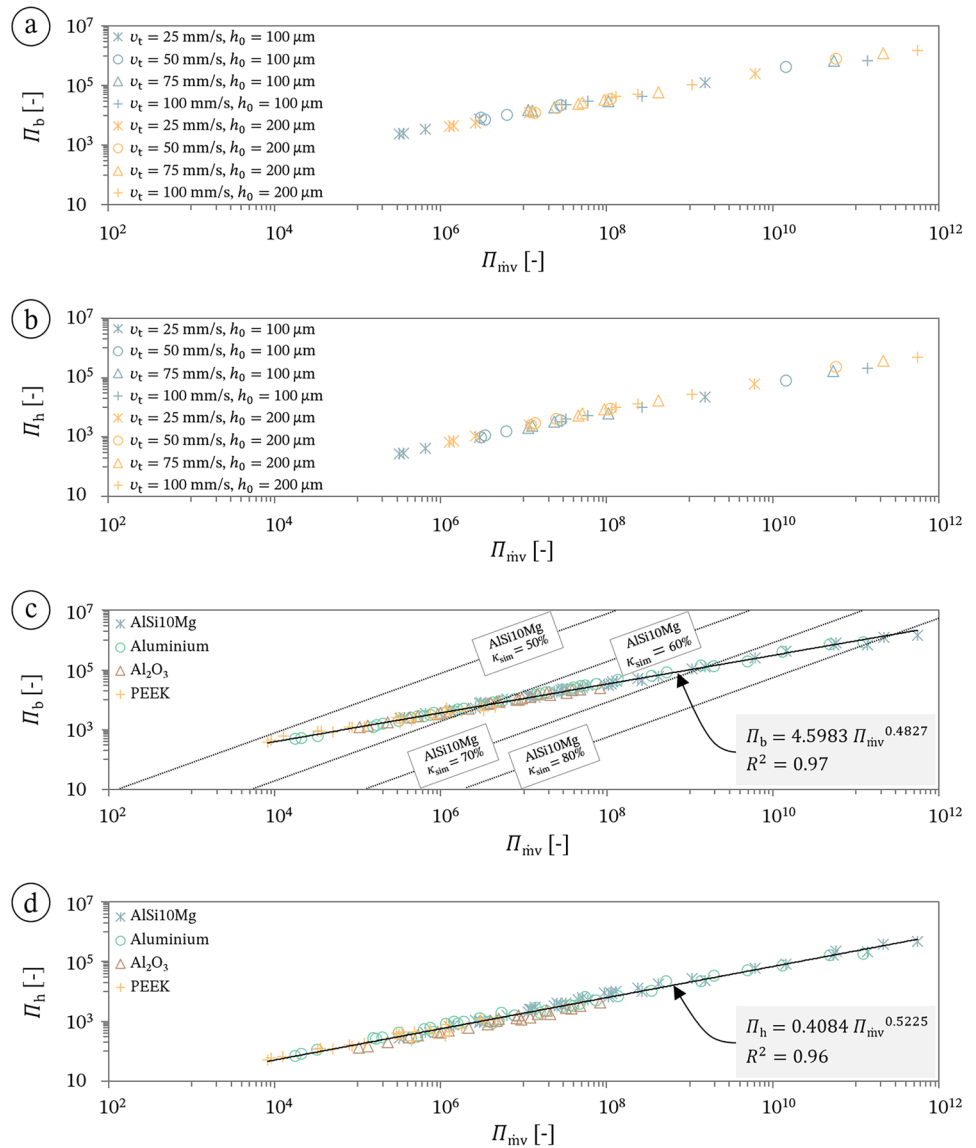


Fig. 9 Correlations between powder track dimensions and powder mass flow rate for **a** the track width and **b** the track height for AlSi10Mg powder, subdivided according to the dispenser translation speed and the distance between the dispenser tip and the substrate, and **c** the track width and **d** the track height, subdivided according to the powder types AlSi10Mg, pure aluminum, Al₂O₃, and PEEK, described with dimensionless quantities



by adjusting the rotational frequency of the ERM, which also affects the deflection amplitude. The relationship is simplified using a spring–mass–damper system as a model, thus it holds

$$\vec{x}_{cir}(t) = \vec{F}_{ex} / \left((k - m_{os} \cdot \omega^2)^2 + (b \cdot \omega)^2 \right)^{0.5} \cdot \sin(\omega \cdot t), \tag{27}$$

where m_{os} represents the oscillating mass, b is the damping coefficient and k is the stiffness of the spring assembly. The excitation force due to static unbalance follows to

$$\vec{F}_{cir}(t) = m_{ERM} \cdot \vec{\omega} \times (\vec{\omega} \times \vec{r}_{ERM}), \tag{28}$$

where m_{ERM} represents the ERM rotating at an eccentricity of \vec{r}_{ERM} . The flow channel inside the VPDD and its tip are

thinly coated with silan, which improves the processability of PEEK powders in particular. However, after processing of Al₂O₃ powder for about 4 h, some wear is visible on the tip (Fig. 8b), which limits its durability. It is assumed that an improvement may be achieved with increased coating thicknesses.

5.3 Physical experiments and integration of simulative results

The results of the physical experiments using the introduced miniature VPDD confirm the correlations $\Pi_b(\Pi_{mv})$ and $\Pi_h(\Pi_{mv})$ derived in Chapter 4 and expand upon the simulative results in Sect. 5.1. This is demonstrated for the correlation of the translational velocity (Fig. 9a, b compared

to Fig. 6a, b) and extended towards powder types of two additional material classes (Fig. 9c, d compared to Fig. 7a, b). As evidenced by the similar regression results, the simulated results are also quantitatively validated as reasonable approximations. This leads to the assumption, that the simulatedly identified relationships between the Péclet number, the void volume fraction (Fig. 7c) and its standard deviation (Fig. 7d) are applicable on physical experiments as well. Consequently, for the application of circularly oscillating VPDD, the previous equations can be summarized as

$$\Pi_b = C_{b1} \cdot \Pi_{\text{mv}}^{C_{b2}}, \quad (29)$$

$$\Pi_h = C_{h1} \cdot \Pi_{\text{mv}}^{C_{h2}}, \quad (30)$$

$$\kappa_{\text{ref}} = C_{k1} \cdot Pe_v^{C_{k2}}. \quad (31)$$

When Eqs. 7, 8, 10, 11, 13, 14 and 20–22 are incorporated, then Eqs. 29–31 give

$$b = \rho_g^{1-C_{b2}} \cdot v_t^{2-3.25 \cdot C_{b2}} \cdot (0.25 \cdot m_{\text{ref}} \cdot (\hat{x} \cdot \omega)^2 / \pi \cdot D_{\text{ref}} \cdot h_0)^{2 \cdot C_{b2} - 1} \cdot v_{\text{ref}}^{0.25 \cdot C_{b2}} / (C_{b1} \cdot \dot{m}^{C_{b2}}), \quad (32)$$

$$h = \rho_g^{1-C_{h2}} \cdot v_t^{2-3.25 \cdot C_{h2}} \cdot (0.25 \cdot m_{\text{ref}} \cdot (\hat{x} \cdot \omega)^2 / \pi \cdot D_{\text{ref}} \cdot h_0)^{2 \cdot C_{h2} - 1} \cdot v_{\text{ref}}^{0.25 \cdot C_{h2}} / (C_{h1} \cdot \dot{m}^{C_{h2}}), \quad (33)$$

$$\kappa_{\text{ref}} = C_{k1} \cdot (v_t^{0.75} \cdot v_{\text{ref}}^{0.25} \cdot \dot{m} \cdot b \cdot \pi \cdot D_{\text{ref}} \cdot h_0 / (0.25 \cdot m_{\text{ref}} \cdot (\hat{x} \cdot \omega)^2))^{C_{k2}}. \quad (34)$$

The coefficients and exponents result from the regression analysis of the simulations (Fig. 7c, d) and physical experiments (Fig. 9c, d), with values as follows: $C_{b1} = 4.5983$; $C_{b2} = 0.4827$; $C_{h1} = 0.4084$; $C_{h2} = 0.5225$; $C_{k1} = 44.092$ und $C_{k2} = 0.0491$. The correlation identified in the simulation for sufficiently flowing AlSi10Mg powder, corresponding to Eq. 31, is plotted in Fig. 9c in the form of lines of equal void volume fraction in order to enable an improved comprehensibility. However, since no clear relationship has been established between the flow properties of the respective powders and the resulting void volume fraction, the iso-lines do not represent a universally applicable formulation and should be interpreted depending on the respective flow properties. For powders with decreased flow properties in comparison to the reference (denoted by the index ref), such as the polygonal PEEK powder [59], a shift of the iso-lines towards lower Π_{mv} -values would be necessary. An analogue shift to Π_{mv} -values would result for materials and powders with improved flow characteristics.

According to these results, the effort required for the application of VPDD in additive manufacturing can be

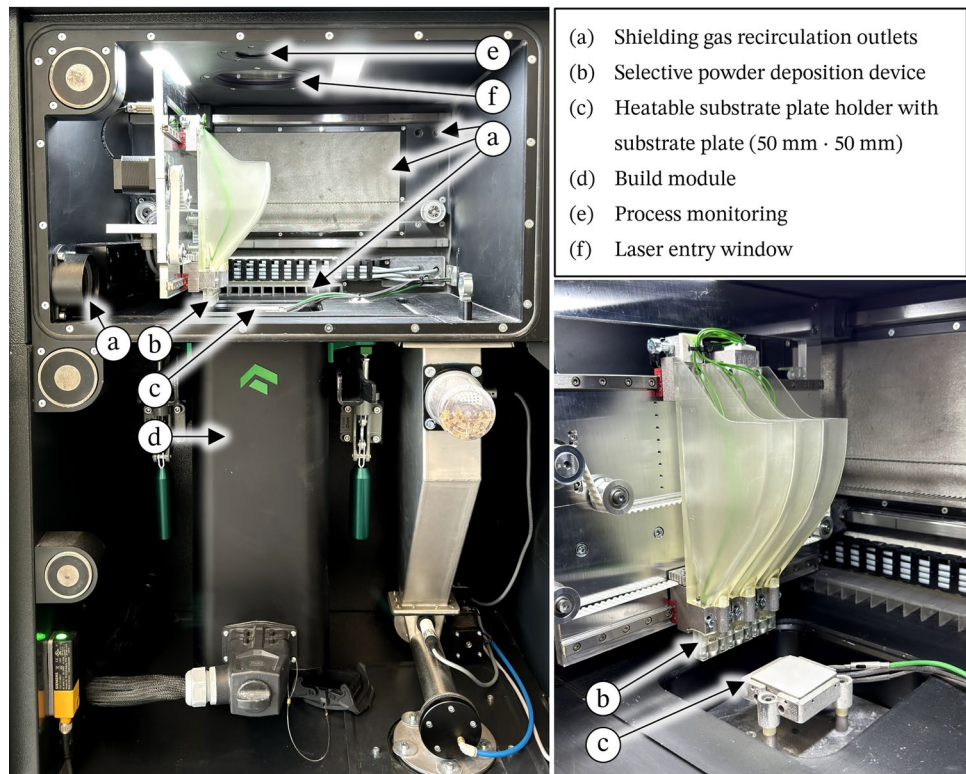
significantly reduced using the identified relationships. Therefore, the prerequisites are physically determined powder properties (ρ_g, m_{ref}) and the mass flow correlation $\dot{m}(E_{\text{os}}, A_1)$, which both can be obtained in experiments with limited effort. Thus, an equation-based parameter adaptation can be performed, involving relationships between process parameters (\dot{m}, f, \hat{x}, v_t), powder properties and the process result ($h, b, \kappa_{\text{cir}}$).

6 Conclusion and outlook

The goal of the presented research was to identify and develop untapped potential for selective powder deposition (SPD) in additive manufacturing. This was achieved by the theoretical deduction and experimental validation of a novel method for the application of vibratory powder deposition devices (VPDD) based on dimensionless quantities using AlSi10Mg, Al, Al₂O₃ and PEEK powders as examples. In this context, the study initially focused on developing a

framework for evaluating the applicability of different SPD approaches. The framework was used to evaluate the applicability of VPDD, aerodynamic powder deposition devices (apdd) and electrostatic powder deposition devices (EPDD) in terms of their applicability and the resulting powder layer quality. It was concluded that the powder layer quality generated by VPDD could be superior to that generated by EPDD and APDD, but potential for further research regarding an improved operability should be explored. This was addressed through a determination of regression functions including three dimensionless quantities derived in this study, which enabled the calculation of control quantities according to the required process results (track width, track height and void volume fraction). The validity of the obtained correlations was first demonstrated using the discrete-element method (DEM) for circular, lateral and partially for axial oscillation of a capillary VPDD. Circular oscillation was identified as the most suitable solution, mainly due to the resulting highest degree of homogeneity and the comparably low void volume fraction. It was, therefore, used to validate the DEM-based findings in reality, using a novel miniature VPDD,

Fig. 10 Laser powder bed fusion machine (One Click Metal MPRINT) with SPD system implementation using the dispenser presented in this study



proving an overall improved applicability and comprehension of this class of SPD devices. The demanding processing of polymers, due in part to their comparatively low density, was overcome using a silane coating on the dispenser and demonstrated using PEEK as an example.

Ultimately, the presented method facilitates a notable improvement for the applicability of VPDD. Moreover, it represents an integrative constituent, which is an appropriate basis for further research efforts in the field of processing multi-material powder beds. This is also aided by the size of the presented VPDD, which benefits the integration of multi-material capabilities into existing equipment (Fig. 10), but requires further size reduction to optimize the operability of such systems. An extension of the method to other frequency and amplitude ranges, different dispenser geometries as well as powder types with differing flow properties is conceivable and could further improve the practicability of the examined approaches.

Acknowledgements The authors gratefully acknowledge the support of Micro-Epsilon Messtechnik GmbH & Co. KG for providing the scanCONTROL 3060-25 sensor used in this study.

Funding Open Access funding enabled and organized by Projekt DEAL.

Data availability All data are already sufficiently disclosed in the manuscript.

Declarations

Conflict of interest On behalf of all the authors, the corresponding author states that there is no conflict of interest associated with this script.

Open Access This article is licensed under a Creative Commons Attribution 4.0 International License, which permits use, sharing, adaptation, distribution and reproduction in any medium or format, as long as you give appropriate credit to the original author(s) and the source, provide a link to the Creative Commons licence, and indicate if changes were made. The images or other third party material in this article are included in the article's Creative Commons licence, unless indicated otherwise in a credit line to the material. If material is not included in the article's Creative Commons licence and your intended use is not permitted by statutory regulation or exceeds the permitted use, you will need to obtain permission directly from the copyright holder. To view a copy of this licence, visit <http://creativecommons.org/licenses/by/4.0/>.

References

1. Dzogbewu TC, de Beer D (2023) Powder Bed Fusion of Multi-materials. *JMMP* 7:15. <https://doi.org/10.3390/jmmp7010015>
2. Mehrpouya M, Tuma D, Vaneker T, Afrasiabi M, Bambach M, Gibson I (2022) Multimaterial powder bed fusion techniques. *RPJ* 28:1–19. <https://doi.org/10.1108/RPJ-01-2022-0014>
3. Koopmann J, Voigt J, Niendorf T (2019) Additive Manufacturing of a Steel-Ceramic Multi-Material by Selective Laser Melting. *Metall and Materi Trans B* 50:1042–1051. <https://doi.org/10.1007/s11663-019-01523-1>

4. Kumke M (2018), *Methodisches Konstruieren von additiv gefertigten Bauteilen*. Dissertation, Springer Fachmedien Wiesbaden, Wiesbaden
5. Mussatto A (2022) Research progress in multi-material laser-powder bed fusion additive manufacturing: a review of the state-of-the-art techniques for depositing multiple powders with spatial selectivity in a single layer. *Results Eng* 16:100769. <https://doi.org/10.1016/j.rineng.2022.100769>
6. Koopmann J (2019), *Multimaterialdruck von integrierten elektrischen Strukturen mittels selektivem Laserschmelzen*. Dissertation, Kassel University Press, Kassel
7. Bai Y, Zhang J, Zhao C, Li C, Wang H (2020) Dual interfacial characterization and property in multi-material selective laser melting of 316L stainless steel and C52400 copper alloy. *Mater Charact* 167:110489. <https://doi.org/10.1016/j.matchar.2020.110489>
8. Schneck M, Horn M, Schmitt M, Seidel C, Schlick G, Reinhart G (2021) Review on additive hybrid- and multi-material-manufacturing of metals by powder bed fusion: state of technology and development potential. *Prog Addit Manuf* 6:881–894. <https://doi.org/10.1007/s40964-021-00205-2>
9. Neirinc B, Li X, Hick M (2021) Powder Deposition Systems Used in Powder Bed-Based Multimetal Additive Manufacturing. *Acc Mater Res* 2:387–393. <https://doi.org/10.1021/accountsmr.1c00030>
10. Vock S, Klöden B, Kirchner A, Weißgärber T, Kieback B (2019) Powders for powder bed fusion: a review. *Prog Addit Manuf* 4:383–397. <https://doi.org/10.1007/s40964-019-00078-6>
11. Le KQ (2020) Computational modeling of selective laser melting process. Dissertation, Nanyang, Singapore
12. Meier C, Fuchs SL, Much N, Nitzler J, Penny RW, Praegla PM, Proell SD, Sun Y, Weissbach R, Schreter M, Hodge NE, John Hart A, Wall WA (2021) Physics-based modeling and predictive simulation of powder bed fusion additive manufacturing across length scales. *GAMM-Mitteilungen* 14:10. <https://doi.org/10.1002/gamm.202100014>
13. Sun Z, Chueh Y-H, Li L (2020) Multiphase mesoscopic simulation of multiple and functionally gradient materials laser powder bed fusion additive manufacturing processes. *Addit Manuf* 35:101448. <https://doi.org/10.1016/j.addma.2020.101448>
14. Shaheen MY, Thornton AR, Luding S, Weinhart T (2021) The influence of material and process parameters on powder spreading in additive manufacturing. *Powder Technol* 383:564–583. <https://doi.org/10.1016/j.powtec.2021.01.058>
15. Ahmed M, Pasha M, Nan W, Ghadiri M (2020) A simple method for assessing powder spreadability for additive manufacturing. *Powder Technol* 367:671–679. <https://doi.org/10.1016/j.powtec.2020.04.033>
16. Averardi A, Cola C, Zeltmann SE, Gupta N (2020) Effect of particle size distribution on the packing of powder beds: a critical discussion relevant to additive manufacturing. *Mater Today Commun* 24:100964. <https://doi.org/10.1016/j.mtcomm.2020.100964>
17. Chen H, Chen Y, Liu Y, Wei Q, Shi Y, Yan W (2020) Packing quality of powder layer during counter-rolling-type powder spreading process in additive manufacturing. *Int J Mach Tools Manuf* 153:103553. <https://doi.org/10.1016/j.ijmactools.2020.103553>
18. He Y, Gardy J, Hassanpour A, Bayly AE (2020) A digital-based approach for characterising spread powder layer in additive manufacturing. *Mater Des* 196:109102. <https://doi.org/10.1016/j.matdes.2020.109102>
19. Meier C, Weissbach R, Weinberg J, Wall WA, Hart AJ (2019) Critical influences of particle size and adhesion on the powder layer uniformity in metal additive manufacturing. *J Mater Process Technol* 266:484–501. <https://doi.org/10.1016/j.jmatprotec.2018.10.037>
20. Haeri S (2017) Optimisation of blade type spreaders for powder bed preparation in Additive Manufacturing using DEM simulations. *Powder Technol* 321:94–104. <https://doi.org/10.1016/j.powtec.2017.08.011>
21. Parteli EJR, Pöschel T (2016) Particle-based simulation of powder application in additive manufacturing. *Powder Technol* 288:96–102. <https://doi.org/10.1016/j.powtec.2015.10.035>
22. Le T-P, Wang X, Davidson KP, Fronda JE, Seita M (2021) Experimental analysis of powder layer quality as a function of feedstock and recoating strategies. *Addit Manuf* 39:101890. <https://doi.org/10.1016/j.addma.2021.101890>
23. Xiang Z, Yin M, Deng Z, Mei X, Yin G (2016) Simulation of forming process of powder bed for additive manufacturing. *J Manuf Sci Eng* 138:081002. <https://doi.org/10.1115/1.4032970>
24. Girnth S, Koopmann J, Klawitter G, Waldt N, Niendorf T (2019) 3D hybrid-material processing in selective laser melting: implementation of a selective coating system. *Prog Addit Manuf* 4:399–409. <https://doi.org/10.1007/s40964-019-00082-w>
25. Anstatt C (2020), *Multimaterialverarbeitung mittels Laserstrahl-schmelzen am Beispiel von metallischen Verbindungen mit der Kupferlegierung CW106C*. Dissertation, München
26. Tang C, Tan JL, Wong CH (2018) A numerical investigation on the physical mechanisms of single track defects in selective laser melting. *Int J Heat Mass Transf* 126:957–968. <https://doi.org/10.1016/j.ijheatmasstransfer.2018.06.073>
27. Al-Jamal OM, Hinduja S, Li L (2008) Characteristics of the bond in Cu–H13 tool steel parts fabricated using SLM. *CIRP Ann* 57:239–242. <https://doi.org/10.1016/j.cirp.2008.03.010>
28. Chianrabutra S, Mellor BG, Yang S (2014) A dry powder material delivery device for multiple material additive manufacturing. In: 2014 International Solid Freeform Fabrication Symposium
29. Stichel T, Laumer T, Amend P (2013) Polymer powder deposition with vibrating capillary nozzles for additive manufacturing. In: Proceedings of the 29th International Conference of the Polymer Processing Society, PPS 2013, AIP, New York, NY, 2013
30. Stichel T, Laumer T, Baumüller T, Amend P, Roth S (2014) Powder layer preparation using vibration-controlled capillary steel nozzles for additive manufacturing. *Phys Procedia* 56:157–166. <https://doi.org/10.1016/j.phpro.2014.08.158>
31. Stichel T, Laumer T, Raths M, Roth S (2018) Multi-material deposition of polymer powders with vibrating nozzles for a new approach of laser sintering. *JLMN* 13:55–62. <https://doi.org/10.2961/jlmn.2018.02.0002>
32. Stichel T, Laumer T, Wittmann P, Amend P, Roth S (2015), Selective deposition of polymer powder by vibrating nozzles for laser beam melting. In: Proceedings of lasers in manufacturing conference, München, 2015
33. Wei C, Sun Z, Chen Q, Liu Z, Li L (2019) Additive manufacturing of horizontal and 3D functionally graded 316L/Cu10Sn components via multiple material selective laser melting. *J Manuf Sci Eng* 141:081014–081021. <https://doi.org/10.1115/1.4043983>
34. Wolff SJ, Wu H, Parab N, Zhao C, Ehmann KF, Sun T, Cao J (2019) In-situ high-speed X-ray imaging of piezo-driven directed energy deposition additive manufacturing. *Sci Rep* 9:962. <https://doi.org/10.1038/s41598-018-36678-5>
35. Wei C, Gu H, Li Q, Sun Z, Chueh Y-H, Liu Z, Li L (2021) Understanding of process and material behaviours in additive manufacturing of Invar36/Cu10Sn multiple material components via laser-based powder bed fusion. *Addit Manuf* 37:101683. <https://doi.org/10.1016/j.addma.2020.101683>
36. Zhang X, Wei C, Chueh Y-H, Li L (2019) An integrated dual ultrasonic selective powder dispensing platform for three-dimensional printing of multiple material metal/glass objects in selective laser melting. *J Manuf Sci Eng* 141:011003. <https://doi.org/10.1115/1.4041427>

37. Boivie K, Karlsen R, van der Eijk C (2006) Material issues of the metal printing process, MPP. In: Proceedings of the 2006 International Solid Freeform Fabrication Symposium, Austin, Texas USA, 2006
38. Foerster J, Michatz M, Binder M, Frey A, Seidel C, Schlick G, Schilp J (2022) Electrostatic powder attraction for the development of a novel recoating system for metal powder bed-based additive manufacturing. *J Electrostat* 115:103641. <https://doi.org/10.1016/j.elstat.2021.103641>
39. Foerster J, Vranjes K, Binder M, Schlick G, Seidel C, Schilp J (2022) Electrophotographic Powder Application for Metal Powder bed based Additive Manufacturing. *Procedia CIRP* 113:353–360. <https://doi.org/10.1016/j.procir.2022.09.142>
40. Kumar AV, Dutta A, Fay JE (2004) Electrophotographic printing of part and binder powders. *Rapid Prototyping J* 10:7–13. <https://doi.org/10.1108/13552540410512480>
41. Stichel T, Brachmann C, Rath M, Dechet MA, Schmidt J, Peukert W, Frick T, Roth S (2020) Electrophotographic multilayer powder pattern deposition for additive manufacturing. *JOM* 72:1366–1375. <https://doi.org/10.1007/s11837-019-03965-z>
42. Stichel T, Laumer T, Amend P, Roth S (2014) Electrostatic multi-material powder deposition for simultaneous laser beam melting. In: Proceedings of the International Conference on Information, Communication and Automation Technologies (ICAT), Wien, 2014
43. van der Eijk C, Asebo O, Mugaas T, Karlsen R, Skjevdal, Boivie k (2005), Metal printing process: a rapid manufacturing process based on xerography using metal powders. In: Proceedings of Materials Science and Technology-Association for Iron and Steel Technology
44. Jones JB (2013) Investigation of laser printing for 3D printing and additive manufacturing. Dissertation, Coventry, United Kingdom
45. Bedoret A, Hick M, Eckes K (2018) BE1024613A1
46. Bareth T, Binder M, Kindermann P, Stapff V, Rieser A, Seidel C (2022) Implementation of a multi-material mechanism in a laser-based powder bed fusion (PBF-LB) machine. *Procedia CIRP* 107:558–563. <https://doi.org/10.1016/j.procir.2022.05.025>
47. Wei C, Li L, Zhang X, Chueh Y-H (2018) 3D printing of multiple metallic materials via modified selective laser melting. *CIRP Ann* 67:245–248. <https://doi.org/10.1016/j.cirp.2018.04.096>
48. Yang SF, Evans JRG (2005) Preparing 3D Functional Gradients for SLS. *MSF* 492–493:749–754. <https://doi.org/10.4028/www.scientific.net/msf.492-493.749>
49. Wei C, Gu H, Zhang X, Chueh Y-H, Li L (2020) Hybrid ultrasonic and mini-motor vibration-induced irregularly shaped powder delivery for multiple materials additive manufacturing. *Addit Manuf* 33:101138. <https://doi.org/10.1016/j.addma.2020.101138>
50. Lu X, Yang S, Evans JRG (2006) Studies on ultrasonic microfeeding of fine powders. *J Phys D Appl Phys* 39:2444–2453. <https://doi.org/10.1088/0022-3727/39/11/020>
51. Lu X, Yang S, Evans JRG (2009) Microfeeding with different ultrasonic nozzle designs. *Ultrasonics* 49:514–521. <https://doi.org/10.1016/j.ultras.2009.01.003>
52. Chueh Y-H, Wei C, Zhang X, Li L (2020) Integrated laser-based powder bed fusion and fused filament fabrication for three-dimensional printing of hybrid metal/polymer objects. *Addit Manuf* 31:100928. <https://doi.org/10.1016/j.addma.2019.100928>
53. Chueh Y-H, Zhang X, Ke JC-R, Li Q, Wei C, Li L (2020) Additive manufacturing of hybrid metal/polymer objects via multiple-material laser powder bed fusion. *Addit Manuf* 36:101465. <https://doi.org/10.1016/j.addma.2020.101465>
54. Fu CH, Guo YB (2014) Three-Dimensional Temperature Gradient Mechanism in Selective Laser Melting of Ti-6Al-4V. *J Manuf Sci Eng* 136:061004. <https://doi.org/10.1115/1.4028539>
55. Jasion GT, Shrimpton JS, Li Z, Yang S (2013) On the bridging mechanism in vibration controlled dispensing of pharmaceutical powders from a micro hopper. *Powder Technol* 249:24–37. <https://doi.org/10.1016/j.powtec.2013.07.027>
56. Wischeropp TM, Emmelmann C, Brandt M, Pateras A (2019) Measurement of actual powder layer height and packing density in a single layer in selective laser melting. *Addit Manuf* 28:176–183. <https://doi.org/10.1016/j.addma.2019.04.019>
57. Khairallah SA, Anderson AT, Rubenchik A, King WE (2016) Laser powder-bed fusion additive manufacturing: Physics of complex melt flow and formation mechanisms of pores, spatter, and denudation zones. *Acta Mater* 108:36–45. <https://doi.org/10.1016/j.actamat.2016.02.014>
58. van der Eijk C, Mugaas T, Karlsen R, Åsebø O, Kolnes Ø, Skjevdal R (2004) Metal printing process development of a new rapid manufacturing process for metal Parts. In: Proceedings of the World PM2004 Conference, Wien, 2004
59. Girth S, Heitkamp T, Wacker C, Waldt N, Klawitter G, Dröder K (2024) Dimensionless quantities in discrete element method: powder model parameterization for additive manufacturing. *Prog Addit Manuf*. <https://doi.org/10.1007/s40964-023-00543-3>
60. DIN EN ISO 4497:2020-10 (2020) Metallpulver - Bestimmung der Teilchengröße durch Trockensiebung. Beuth Verlag GmbH, Berlin
61. Hertz HR (1882) Über die Berührung fester elastischer Körper und über die Härte, vol 11. Verhandlung des Vereins zur Beförderung des Gewerbefleißes, Berlin
62. Mindlin RD (1949) Compliance of elastic bodies in contact. *J Appl Mech* 16:259–268. <https://doi.org/10.1115/1.4009973>
63. Tsuji Y, Tanaka T, Ishida T (1992) Lagrangian numerical simulation of plug flow of cohesionless particles in a horizontal pipe. *Powder Technol* 71:239–250. [https://doi.org/10.1016/0032-5910\(92\)88030-L](https://doi.org/10.1016/0032-5910(92)88030-L)
64. Johnson KL, Kendall K, Roberts AD (1971) Surface energy and the contact of elastic solids. *Proc R Soc Lond A* 324:301–313. <https://doi.org/10.1098/rspa.1971.0141>
65. Buckingham E (1914) On physically similar systems; illustrations of the use of dimensional equations. *Phys Rev* 4:345–376. <https://doi.org/10.1103/physrev.4.345>
66. Großmann A, Felger J, Frölich T, Gosmann J, Mittelstedt C (2019) Melt pool controlled laser powder bed fusion for customised low-density lattice structures. *Mater Des* 181:108054. <https://doi.org/10.1016/j.matdes.2019.108054>
67. Naderi M, Weaver J, Deisenroth D, Iyyer N, McCauley R (2023) On the fidelity of the scaling laws for melt pool depth analysis during laser powder bed fusion. *Integr Mater Manuf Innov* 12:11–26. <https://doi.org/10.1007/s40192-022-00289-w>
68. Yang Y, Großmann A, Kühn P, Möllene J, Kropholler L, Mittelstedt C, Xu B-X (2022) Validated dimensionless scaling law for melt pool width in laser powder bed fusion. *J Mater Process Technol* 299:117316. <https://doi.org/10.1016/j.jmatprotec.2021.117316>
69. Vo TT, Nezamabadi S, Mutabaruka P, Delenne J-Y, Radjai F (2020) Additive rheology of complex granular flows. *Nat Commun* 11:1476. <https://doi.org/10.1038/s41467-020-15263-3>
70. Midi GDR (2004) On dense granular flows. *Eur Phys J E Soft Matter* 14:341–365. <https://doi.org/10.1140/epje/i2003-10153-0>

Publisher's Note Springer Nature remains neutral with regard to jurisdictional claims in published maps and institutional affiliations.